Investigating the influence of freezing rate and frozen storage conditions on a model sponge cake using synchrotron X-rays micro-computed tomography

Amira Zennoune, Hayat Benkhelifa, Frédéric Flin, Fatou-Toutie Ndoye, Jonathan Perrin, Timm Weitkamp, Mario Scheel, Pierre Latil, Christian Geindreau

Investigating the influence of freezing rate and frozen storage conditions on a model sponge cake using Synchrotron X-rays micro-computed tomography

Amira Zennoune [1,2], Pierre Latil [3], Frederic Flin [3], Jonathan Perrin[4], Timm Weitkamp [4], Mario Scheel[4], Christian Geindreau [5], Hayat Benkhelifa [1,2] and Fatou-Toutie Ndoye [1]*

[1] Université Paris-Saclay, INRAE, UR FRISE, F-92761 Antony, France; amira.zennoune@inrae.fr; fatou-toutie.ndoye@inrae.fr
[2] Université Paris-Saclay, INRAE, AgroParisTech, 75005 Paris, France, hayat.benkhelifa@agroparistech.fr
[3] Univ. Grenoble Alpes, Université de Toulouse, Météo-France, CNRS, CNRM, Centre d'Etudes de la Neige, Grenoble, France; pierre.latil@meteo.fr; frederic.flin@meteo.fr
[4] Synchrotron SOLEIL, Gif sur Yvette, France; timm.weitkamp@synchrotron-soleil.fr; mario.scheel@synchrotron-soleil.fr; jonathan.perrin@synchrotron-soleil.fr
[5] Université Grenoble Alpes, Grenoble INP, 3SR, CNRS, Grenoble, France; christian.geindreau@3sr-grenoble.fr
* Correspondence: fatou-toutie.ndoye@inrae.fr

Abstract

Synchrotron X-rays micro-computed tomography was applied to visualize and quantify 3D ice crystal changes into a model sponge cake after freezing and subsequent frozen storage. Model sponge cake samples were submitted to two different freezing rates (fast: 17.2 °C min^{-1} and slow: 0.3 °C min^{-1}), then stored at constant and fluctuating temperatures over a two weeks period. 3D images were acquired at frozen state thanks to a thermostated cell (CellStat) and processed using a grey level based segmentation method. Image analysis revealed that the ice volume fraction is conserved during storage but ice crystal size and location change whatever the freezing rate and the storage conditions. Maximum local thicknesses increase both inside (from 20 µm to 50 µm) and outside (from 47µm to 70µm) the matrix during the fourteen days storage period. Both specific surface areas between starch and ice ($SSA_{ice/starch}$) and between air and ice ($SSA_{air/ice}$) also evolve with storage duration: $SSA_{ice/starch}$ decreases up to −30% while $SSA_{air/ice}$ increases up to +13% depending on the freezing rates and the storage conditions. These results highlighted that, during storage, ice crystals evolve according to two different mechanisms depending on the freezing rate: fast freezing leads to a local redistribution of water both within the starch matrix and within the pores, while slow freezing results in both local redistribution within the starch matrix and water migration towards the pores. In addition, stable storage temperatures favor local water redistribution whereas water migration from the starch matrix towards the pores was greater in the case of fluctuating storage temperatures. This study shows that freezing and frozen storage conditions have a synergistic effect on the microstructure evolution of sponge cake due to recrystallization phenomena.

Keywords: Freezing rate; Frozen storage; Sponge cake; Microstructure; Recrystallization, Synchrotron X-ray micro-computed tomography.

I. Introduction

Sponge cakes are used as a base product in the manufacture of a wide variety of desserts. To meet the high demand of the market, large quantities are produced, but sponge cakes have a

limited shelf life due to physicochemical changes and microbial deterioration. Therefore, sponge cakes are frozen just after baking and stored until their distribution in retail stores where they are thawed and decorated. Freezing and frozen storage have the advantage to preserve the sponge cake quality and to extend their shelf life. However, the evolution of the microstructure (pore and ice crystal size and morphology) after the formation and growth of ice crystals could induce physicochemical changes that could impair the sponge cake organoleptic quality.

During freezing, the temperature of the product is lowered, and water is transformed into ice crystals by crystallization (nucleation and ice crystal growth). The freezing rate controls the crystallization mechanism, which consequently determines the number of ice crystals as well as their size and distribution through the matrix. Many authors reported that fast freezing leads to the formation of a large number of small ice crystals evenly distributed in the matrix. Unlike fast freezing, slow freezing leads to the formation of bigger ice crystals that can damage the microstructure of the food (Mousavi et al. 2005, Ban et al. 2016, Mulot et al. 2019). In the case of porous food, a recent study performed on model sponge cake has shown that fast freezing leads to the formation of the majority of ice inside the matrix while slow freezing results in ice mostly formed at the pore surface (Zennoune et al. 2021).

In subsequent frozen storage, the microstructure of frozen food continues to evolve, especially for long term storage. This evolution is due to ice recrystallization: the system tends naturally to lower the surface free energy of the whole ice phase by ice crystal resizing and redistribution. Larger and shape-regular ice crystals, which are thermodynamically more stable, are favored at the expense of small and shape-irregular ice crystals. This leads to an increase of the average size of ice crystals and to a decrease of their number (Donhowe and Hartel 1996, Hartel 1998, Hagiwara et al. 2006). Several recrystallization mechanisms were identified. Among them, migratory recrystallization, also known as Ostwald ripening is recognized as one of the most prominent in frozen foods. Ostwald ripening is characterized by the gradual detachment of water molecule from the surface of smaller ice crystals, followed by water molecules diffusion and redeposition onto large ice crystals. Consequently, small ice crystals tend to disappear while larger ones become bigger (Pronk et al. 2005). Other recrystallization mechanisms that can take place in frozen foods are isomass recrystallization (rounding of edges and sharp features of ice crystals with irregular shape to minimize their surface free energy) and accretive recrystallization (merging of two crystals in close proximity to form one large crystal). Isomass recrystallization results in crystals with more regular shape while keeping their number constant. Accretive and migratory recrystallization lead to an increase of ice crystal size and a reduction of ice crystal number (Hartel, 2018). Ice recrystallization occurs slowly during long-term frozen storage at constant temperature but is greatly enhanced by temperature fluctuations due to the normal on/off operation of the freezer compressor or to poor practices in the cold chain, as often encountered. Therefore, it is of great importance to properly control the temperature during storage and distribution in order to maintain the quality of the frozen products and to minimize product losses.

In the specific case of porous foods, the presence of air greatly influences the crystallization and recrystallization phenomena. Indeed, freezing and frozen storage involve simultaneously

heat and water transfer, which are highly related to pore number, size, connectivity and surface. Pham (2006) reported in his review that water diffusion is accelerated by the presence of pores. During freezing, conductive heat transfer is driven by the temperature gradient between the cold surface and the product core. Diffusive water transfer is controlled by the water vapor pressure gradient between the surrounding air and the product surface. When porous foods are frozen, these gradients are also created at the pore scale resulting in water diffusion from the matrix towards the pores where water evaporates. Once the freezing point is reached, the supersaturated water vapor condenses into ice at the pore surface while liquid water crystallizes mainly into the matrix. This phenomenon is commonly called evapo-condensation (Pham 2006). This mechanism is in line with our recent findings on ice formation in both pores and matrix during model sponge cake freezing (Zennoune et al. 2021). Formation of ice crystals is accompanied by both volumetric expansion and sponge cake dehydration that may alter the porous microstructure, which is highly related to the product quality.

During frozen storage of porous foods, concomitant heat and water transfers still occur. It is mainly characterized by recrystallization phenomena (Ostwald ripening) where both melting diffusion-refreezing for the liquid phase and sublimation diffusion-condensation for the vapor phase take place in the matrix and in the pores, respectively. It results in ice crystal growth and further microstructural changes that may ultimately deteriorate the product quality. It is obvious that the final quality of the frozen product is related to the coupling of both freezing and frozen storage processes. Even though the close relationship between porous/crystalline microstructural changes and the quality of frozen porous products was established (Bárcenas et al. 2004, Baier-Schenk et al. 2005, Yi and Kerr 2009, Díaz-Ramírez et al. 2016), a detailed understanding of the mechanisms implemented at pore and ice crystal scale during a combined freezing and frozen storage process is still needed. The rare studies reported in the literature have focused on either freezing (Lucas et al. 2005, Chen et al. 2012) or frozen storage (Chen et al. 2013, Eckardt et al. 2013). Furthermore, these studies were devoted to bread. Silvas-García et al. (2014) have investigated the coupled effect of freezing rate and storage time on bread dough stability and bread quality without characterizing the microstructure. To our knowledge, the literature does not report any study describing the combined effect of freezing and frozen storage on the microstructural changes of porous foods and particularly of sponge cake. Very few works were conducted on frozen sponge cake (Díaz-Ramírez et al. 2016, Van Bockstaele et al. 2021, Zennoune et al. 2021). Díaz-Ramírez et al. (2016) have shown a correlation between microstructure changes and quality attributes of sponge cake stored at −23 °C for 6 months. Recently, Van Bockstaele et al. (2021) have rather investigated sensory and textural properties of frozen sponge cake stored at short-term period. The first work investigating the effect of freezing rate on porous and crystalline microstructure of frozen sponge cake was reported by our team (Zennoune et al. 2021). The authors succeeded in characterizing the evolution of pores and ice crystals in a model sponge cake using synchrotron X-ray micro-computed tomography (X-ray µCT) on products in the frozen state.

Imaging methods could be useful and reliable for the assessment and understanding of the microstructure of frozen products. Microscopy has long been the most commonly used

technique to visualize the effect of freezing and frozen storage on the structure of food products (Bevilacqua et al. 1979, Esselink et al. 2003, Baier-Schenk et al. 2005, Vicent et al. 2019). It includes light microscopy, which requires a very thin sample of the food product and several preliminary chemical preparation steps (fixing, coating, staining) in order to enhance the contrast (Alizadeh et al. 2007, Anese et al. 2013). Transmission and scanning electron microscopy offer higher resolution than light microscopy but also require intensive sample preparation such as freeze-drying for contrast enhancement. These preliminary preparation steps are tedious and likely to alter the microstructure of the product resulting in measurement artefacts. More reliable results can be obtained using cryo-scanning electron microscopy (cryo-SEM), which involves less cumbersome and damaging preparation steps (Chassagne-Berces et al. 2009, Mulot et al. 2019). Cryo-SEM was used to study porous foods like bread dough and bread (Bárcenas and Rosell 2006) and model sponge cake (Zennoune et al. 2021). However, all these microscopy methods provide 2D images which depend on the selected cutting plane. In addition, these 2D images do not afford sufficiently quantitative information that are representative of the entire volume of the product studied.

3D imaging techniques such as X-ray µCT can overcome these limitations. X-ray µCT is a reliable method based on the measurement, at microscopic spatial resolution, of the intensity profile of an X-ray beam transmitted through the sample, which depends on the material characteristics (density, thickness and atomic number). The technique is increasingly used to visualize and quantify the characteristics of frozen food products (Mousavi et al. 2005, Ullah et al. 2014, Vicent et al. 2016, Mulot et al. 2019, Masselot et al. 2021). However, most of the studies so far have focused on the visualization of frozen foods at ambient temperature after freeze-drying (Mousavi et al. 2007, van Dalen et al. 2013, Kobayashi et al. 2014, Zhao and Takhar 2017). These studies assumed that voids created after freeze-drying represent ice crystals. But, freeze-drying may imply shrinkage, which is likely to modify the microstructure, resulting in inconclusive results (Voda et al. 2012). Freeze-drying can be avoided when the product is scanned in the frozen state. This is possible when using a cooling cell as illustrated by several works on frozen food products (van Dalen et al. 2009, Pinzer et al. 2012, Medebacha et al. 2013, Vicent et al. 2017, Mulot 2019, Vicent et al. 2019, Masselot et al. 2021), and other porous frozen materials or systems such as snow (Calonne et al. 2014, Calonne et al. 2015) or ice particles (Haffar et al. 2021, Haffar et al. 2022). In this way, the non-invasive and non-destructive nature of X-ray µCT can be fully taken advantage of. However, these works were performed using laboratory scale X-ray µCT, which cannot always offer sufficiently contrasted images and high resolution for a category of products such as sponge cake. Indeed, sponge cake has a complex microstructure comprising both macropores and micropores requiring high resolution for a consistent and complete characterization. Recently, our team studied the effect of freezing rate on the microstructure of a frozen model-based sponge cake (Zennoune et al. 2021). A thermostated cell (CellStat) (Calonne et al. 2014) was used on the synchrotron µCT beamline ANATOMIX at Synchrotron SOLEIL, the French national synchrotron light source in Gif-sur-Yvette, France (Weitkamp et al. 2017). This study demonstrated that the use of synchrotron can greatly enhance the visibility and discrimination of low contrasted materials in

addition to high resolution, allowing to detect better small features (ice crystals and micropores).

The present paper aims to study the combined impact of freezing rate and frozen storage conditions on the microstructure of a model sponge cake using X-ray µ-CT at high spatial resolution. The samples were frozen at two different freezing rates and each of them were stored for two weeks at two different conditions (with and without temperature fluctuations). The model sponge cake samples were scanned at the ANATOMIX beamline using the thermostated cell CellStat to allow observation in the frozen state. The three phases (air, ice and cake matrix) of the frozen samples were segmented using an image processing method previously developed (Zennoune et al. 2021). The coupled effect of freezing rate and frozen storage was then discussed based on volume fractions of each phase, ice local thickness, ice location and shape characterizations.

II. Materials and methods

II.1. Sponge cake preparation, sampling and freezing

The model sponge cake was prepared using the formulation developed by Bousquières (2017) as described in Zennoune et al. (2021). The main ingredients are:

- Native corn starch (Cargill, Minneapolis, MN, USA): 36.55 % (water content about 11%);
- Methylcellulose (MC) (Dow Chemical, Midland, MI, USA), type SGA7C, 0.46 %;
- Hydroxypropylmethylcellulose (HPMC) (Dow Chemical, Midland, MI, USA), type K250M: 0.35 %;
- Ultrapure water: 62.64 %.

Aluminum molds ($10 \times 6 \times 3$ cm^3) were filled with 60 g of dough and then baked in an electric oven (Whirlpool, Benton, IL, USA) for 30 min at 170 °C. After baking, the sponge cakes were left at room temperature for 45 min before being wrapped in waterproof plastic bags and sealed to be stored in a refrigerator at 5 °C until the sampling step.

For the imaging experiments, cubic samples (of 6 mm side) were cut in the crumb and placed in sample holders made with polymethyl methacrylate (PMMA) and copper (Figure 3) before freezing and storage. This sampling was performed in a thermo-hygroscopic chamber at 20 °C and 80% of relative humidity to avoid sponge cake dehydration during handling.

The prepared samples, mounted on their sample-holders, were frozen in the lab (FRISE, INRAE, Antony, France), before the imaging experiments, at two different freezing rates:

- Fast freezing (17.2 °C min^{-1}) using an air blast freezer,
- Slow freezing (0.3 °C min^{-1}) using a static chest freezer

II.2. Frozen storage conditions and analysis time points

For both freezing conditions (see Table 1), the frozen samples were stored under two thermal conditions, before the imaging experiments:

- Stable storage at −20 ± 0.1°C: using a static chest freezer equipped with an electronic

temperature controller with one set point (Eliwell WM961, Villeneuve la Garenne, France). The samples were placed into a 3 cm thick expanded polystyrene box for insulation in order to attenuate the temperature fluctuations related to the on/off operation of the refrigeration system.

- Fluctuating storage between −20 ± 0.1 °C and −5 ± 0.01 °C: using two different static chest freezers. The samples were held during 23 hours in the first freezer, set at −20 ± 0.1 °C and then moved to the second freezer set at −5 ± 0.01 °C for 1 hour each day during a two-week storage period. The fluctuating storage temperature is schematized in Figure 1.

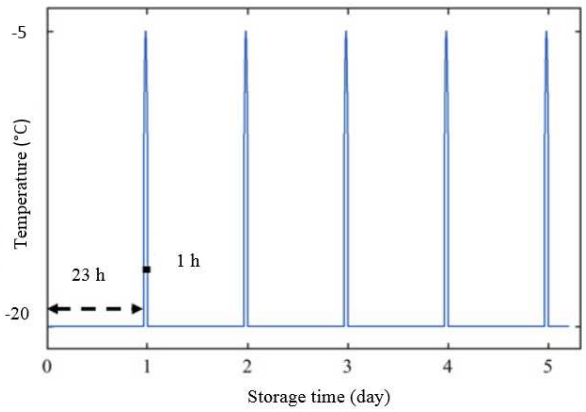

Figure 1: *Schematic representation of the dynamic change of storage temperatures.*

The stable storage temperature condition intends to reproduce perfectly controlled storage conditions of frozen foods in a cold room or in a freezer with no door opening. By contrast, the fluctuating storage was designed to make it possible to study the effect of poor practices that can be encountered through the cold chain. At −5 °C, the sponge cake is still in the phase change plateau as can be seen in the freezing curve shown in Figure 2 and is likely to melt partially. Consequently, the scenario of dynamic change of storage temperature between −20 °C and −5 °C may allow to accelerate moisture migration and ice redistribution (Vicent et al. 2019).

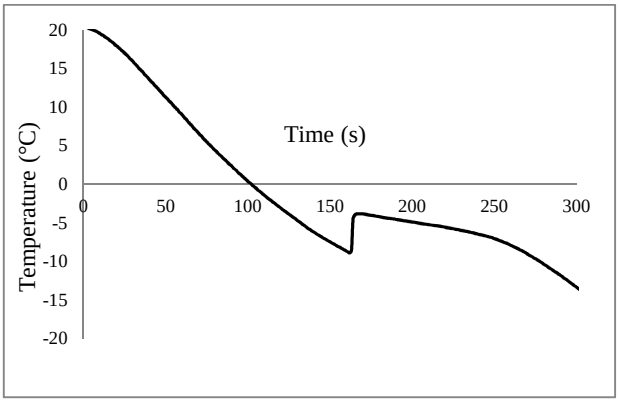

Figure 2 : *Core temperature kinetic during sponge cake freezing.*

As summarized in Table 1, combining the two freezing rates and the two storage conditions gives rise to four different thermal history scenarios. Three analysis time points were set: just after freezing (t_0), after 7 days of storage (t_7) and after 14 days of storage (t_{14}). Analyses at t_0

were performed for each freezing rate. Four replicates were performed for each scenario and each analysis time point, corresponding to a total of 40 samples as shown in Table 1.

Table 1: *Number of analyzed samples per condition.*

Time point	Fast freezing at 17.2 °C min^{-1}		Slow freezing at 0.3 °C min^{-1}	
	Stable storage at −20°C	Fluctuating storage between −20°C and −5°C	Stable storage at −20°C	Fluctuating storage between −20°C and −5°C
t_{14}	4	4	4	4
t_7	4	4	4	4
t_0	4		4	

II.3. Thermo-physical properties of the model sponge cake

The thermo-physical properties of the model sponge cake are summarized in Table 2. All the properties were determined as described by Zennoune et al. (2021). The authors have verified the reproducibility of the model sponge cake based on its thermo-physical properties (porosity, density and water content). They reported that the sponge cake prepared in this way can be considered as a model product that represents porous products.

Table 2: *Sponge cake thermo-physical properties.*

Sponge cake apparent density (kg/m^3)	Porosity (%)	Water content (%)	Freezing point (°C)	Freezable water content (%)
392 ± 15	56 ± 2	60 ± 1.5	−0.52 ± 0.09	44 ± 5.3

The porosity of the sponge cake before freezing was calculated based on the density values (apparent density and batter theoretical density without air, which was found to be equal to 899 kg/m^3) as explained by Zennoune et al. (2021). The mean value of 56 % is close to that found by Roca et al. (2006), where porosities were between 52 % and 86 %. One must keep in mind that porosity of a sample is the combination of the bakery process and the randomness of the sampling. During baking, sponge cake dough containing initially 75 % of water loses nearly 20 % of its moisture content. Indeed, the water content measured after baking was about 60%, but the freezable water was about 44 % as shown by differential scanning calorimetry measurements (Zennoune et al. 2021).

II.4. Synchrotron X-ray micro-tomography imaging acquisition and processing

II.4.1. Thermostated Cell

The thermostated cell CellStat, initially developed for snow (Calonne et al. 2014, Haffar et al. 2021), was used to analyze the frozen microstructure of model sponge cake samples under the synchrotron X-ray µCT environment constraints (Figure 3). It helps to maintain the sample at the frozen state by means of *(i)* a Peltier module, set at a temperature of –36 °C, on which the copper sample holder is placed, *(ii)* a continuous dry and cold air circulation around the sample and *(iii)* a heat exchanger for heat dissipation at the warm side of the Peltier module. Additional details are available in the works of Haffar et al. (2021) and Zennoune et al. (2021). The samples were stored in a freezer set to –30 °C and placed close to the experimental setup, thus ensuring nearly constant thermal conditions.

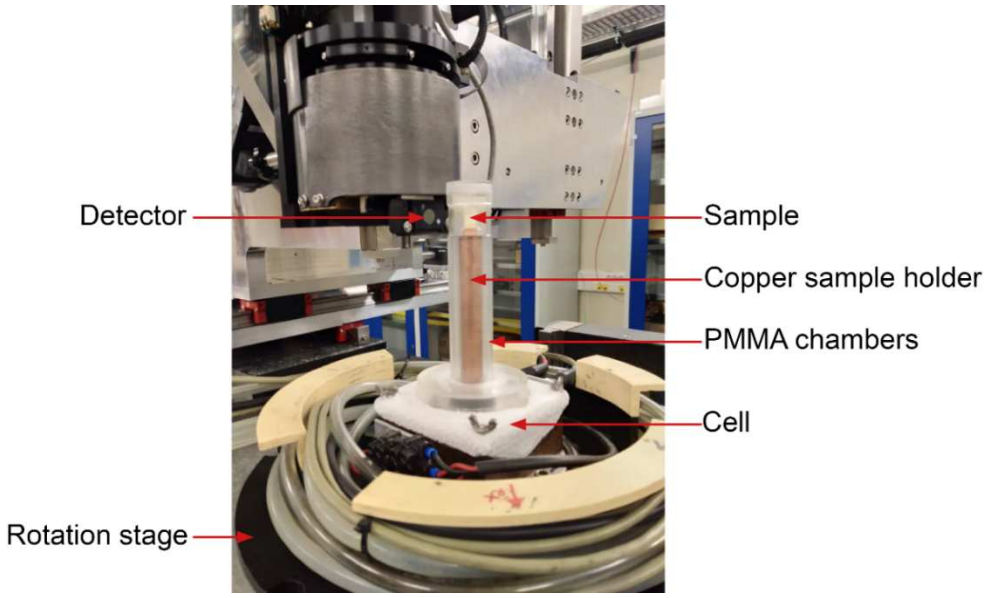

Figure 3: *CellStat installed on the ANATOMIX beamline (Synchrotron SOLEIL, Gif-sur-Yvette, France).*

II.4.2. 3D Image acquisition

The X-ray micro-computed tomography measurements were made at the beamline ANATOMIX of Synchrotron SOLEIL in a campaign that lasted three days. The system operation parameters were optimized as previously described by Zennoune et al. (2021) so as to yield good contrast between the sponge cake constituents at the voxel size of 0.65 µm. A filtered polychromatic "white" beam with a central photon energy around 30 keV was used; the distance between sample and detector was 30 mm. For each volume scan, 2000 projections were taken over an angular range of 180° in continuous rotation. The total time for each scan was about 5 minutes. For each sample, four scans were acquired at different heights giving a total height of the reconstructed volume of 5 mm for a diameter of 1.3 mm. Figure 4 shows typical reconstructed slices of an unfrozen sample (Figure 4A) and a frozen sample (Figure 4B). In that second case, the three components or phases, i.e. air (in black), ice (in grey) and starch (in light grey), are clearly visible.

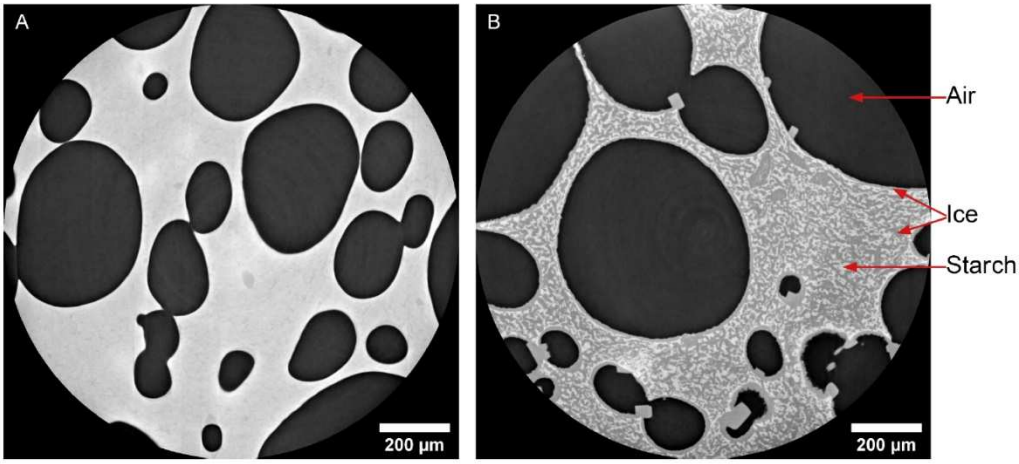

Figure 4: *X-ray µCT slices of (A) unfrozen and (B) frozen model sponge cake samples.*

II.4.3. Image processing

Images were processed according to the methodology described by Zennoune et al. (2021). Firstly, the 3D volumes of size 2048×2048×2048 voxels (corresponding to 1.3×1.3×1.3 mm^3) were reconstructed with PyHST2 software (Mirone et al. 2013) using a Paganin filter (Paganin et al. 2002). The images were then segmented using the Fiji software according to the procedure resumed in Figure 5. It is based on the global grey level threshold of the 3 phases (air, ice, starch) by applying the Otsu multi-thresholding methodology (Otsu 1979) and taking advantage of the good image contrast between the constituents. This segmentation is followed by a combination of morphological (3D closing) and logical (not/and)
operations to distinguish:

- The ice volume which is mainly at the air interface (called “ice outside” the matrix)
- The ice volume which is mainly blended with the starch phase (called “ice inside” the matrix).

The result of the procedure is then a labeled 3D image as depicted in Figure 5, which can be used to compute microstructural descriptors.

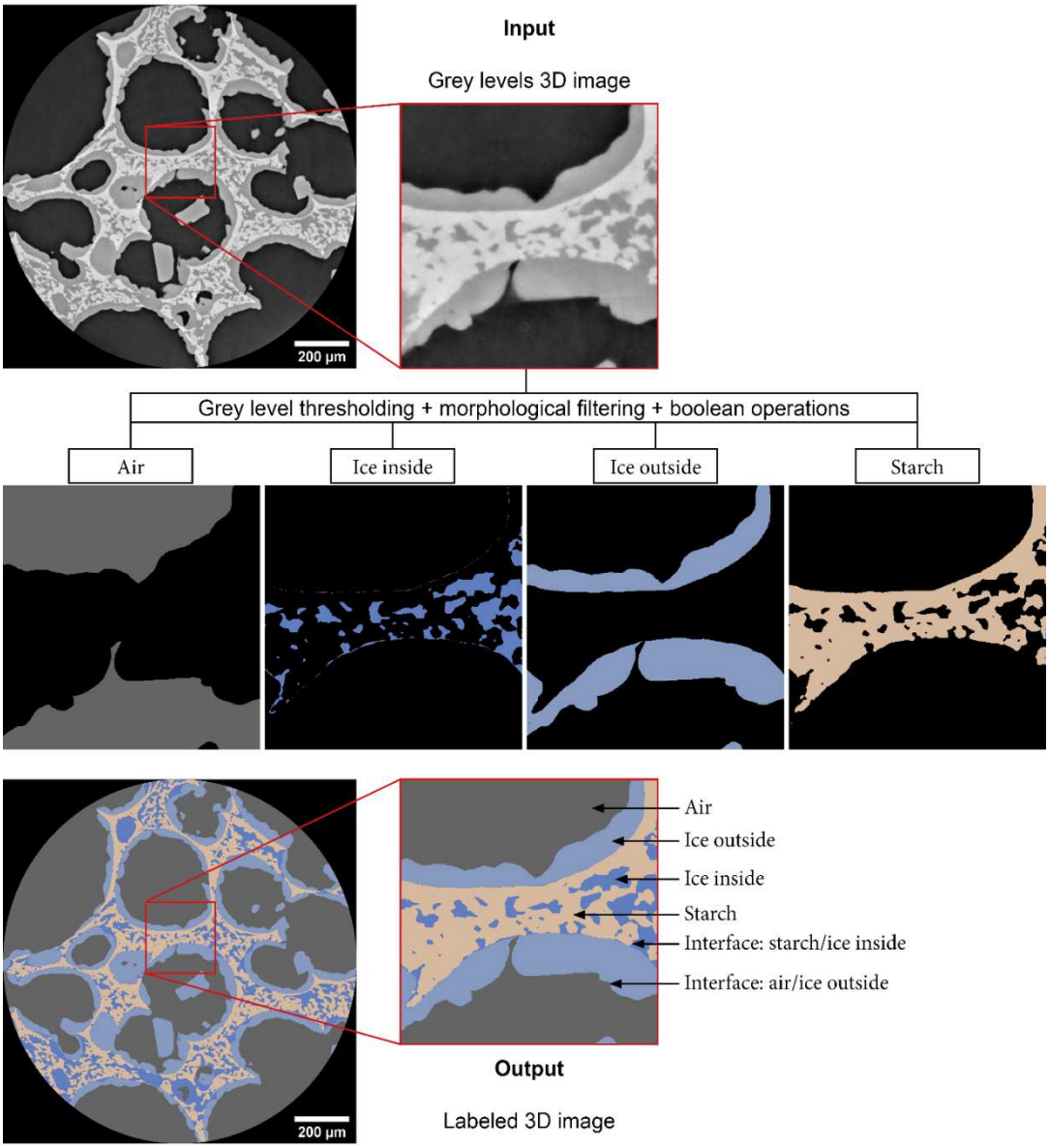

Figure 5: *Image segmentation procedure.*

II.4.4. Microstructural description

To describe the microstructure of the different samples, the following parameters were computed from 3D labeled images:

- The air volume fraction or porosity :

$$\varphi_{\text{air}} = \frac{V_{\text{air}}}{V_{\text{total}}} \quad (1)$$

where $V_{\text{total}} = V_{\text{air}} + V_{\text{ice}} + V_{\text{starch}}$ is the total analyzed volume, V_{air}, $V_{\text{ice}} = V_{\text{ice inside}} + V_{\text{ice outside}}$ and V_{starch} are the volumes of air, ice, ice inside and outside the matrix, and starch, respectively. They are calculated using a classical voxel counting algorithm implemented in Fiji software (Schindelin et al., 2012).

- The ice fraction in the solid phase (without the air),

$$\varphi_{\text{ice}} = \frac{V_{\text{ice}}}{V_{\text{ice}} + V_{\text{starch}}} \quad (2)$$

- The volume fraction of the ice inside ,

$$\varphi_{\text{ice inside}} = \frac{V_{\text{ice inside}}}{V_{\text{ice}} + V_{\text{starch}}} \quad (3)$$

- The specific surface area (*SSA*) of the ice/air interface, defined as

$$SSA_{\text{ice/air}} = \frac{S_{\text{ice/air}}}{V_{\text{total}}} \quad (4)$$

where $S_{\text{ice/air}}$ is the surface area of the air/ice interface (Figure 5) and is computed using the dedicated air/ice tool in (Legland et al. 2016).

- The specific surface area (*SSA*) of the ice/starch interface, defined as

$$SSA_{\text{ice/starch}} = \frac{S_{\text{ice/starch}}}{V_{\text{total}}} \quad (5)$$

where $S_{\text{ice/starch}}$ is the surface area of the air/starch interface (Figure 5).

- The local thickness distributions of ice inside and outside the matrix (Schindelin et al. 2012): it represents the diameter of the largest sphere at a given point that can fit inside the object and containing the given point. It depicts the characteristic dimensions of the ice phases (inside and outside).

II.4.5. Statistical analysis

A statistical analysis based on the analysis of variance (ANOVA) method (Brownlee 1965) was performed to study the significance of the combined effect of freezing rate and frozen storage conditions on model sponge cake microstructure evolution during freezing and storage. The Tukey Kramer test for multiple range comparisons ($p < 0.05$) was used to identify the difference between the measured mean values for volume fractions and *SSA*.

III. Results

III.1. Qualitative analysis

Figure 6 presents synchrotron X-ray micro-computed tomography images (horizontal slices) of the model sponge cake (air in grey, ice outside the matrix in light blue, ice inside the matrix in dark blue and starch in brown) obtained after fast freezing (Figures 6A1 to 6A5) and slow freezing (Figures 6B1 to 6B5). It shows typical microstructure evolution of model sponge cake with storage duration for the four storage scenarios applied (fast freezing/stable storage, fast freezing/fluctuation storage, slow freezing/stable storage; slow freezing/fluctuating storage).

III.1.1. Initial state t_0

Figures 6A1 and 6B1 describes microstructures obtained just after freezing (t_0) at fast and slow freezing, respectively. The corresponding 3D visualizations are shown in Figures 7A1 and 7B1 It can be seen that:

- fast freezing leads to small ice objects homogeneously distributed inside the matrix and to a thin layer of ice that is formed at the air interface;
- slow freezing leads to a thick ice layer at the air interface and larger ice objects heterogeneously distributed inside the matrix.

The physical phenomena that led to such microstructure were explained in our previous research article (Zennoune et al. 2021) and are reported in section IV.

III.1.2. Effect of storage conditions

For the case of fast freezing, Figures 6A1 to 6A3 show the typical microstructures of samples after 0, 7 and 14 days of stable storage, respectively. Figures 6A4 and 6A5 show typical microstructures obtained in the fluctuating storage conditions for 7 and 14 days of storage duration, respectively. Figures 7A1 and 7A5 represents the 3D visualizations of images shown in Figures 6A1 (fast freezing, t_0) and 6A5 (fast freezing, fluctuating storage temperature t_{14}), respectively. The comparison between these figures shows that:

- The ice and starch structures are coarser at t_7 and t_{14} than at t_0 for both stable and fluctuating storage conditions
- The ice layer at the air/starch interface is thicker at t_7 and t_{14} than at t_0,
- There are no visible significant differences of the microstructure between stable and fluctuating storage.

In the case of slow freezing, 2D images (Figures 6B1 to 6B5) as well as 3D visualizations, (Figures 7B1 and 7B5) bring the following comments:

- The ice and starch structures are coarser at t_7 and t_{14} than at t_0 for both stable and fluctuating storage conditions
- The ice layer at the air/starch interface is slightly thicker at t_7 than at t_0 and t_{14},
- Visually, there are no significant differences of the microstructure between stable and fluctuating storage.

All these results could be explained by ice redistribution and water migration during storage as will be discussed in section IV. However, it is worth noting that the qualitative analysis requires a complementary quantitative characterization to establish reliable conclusions.

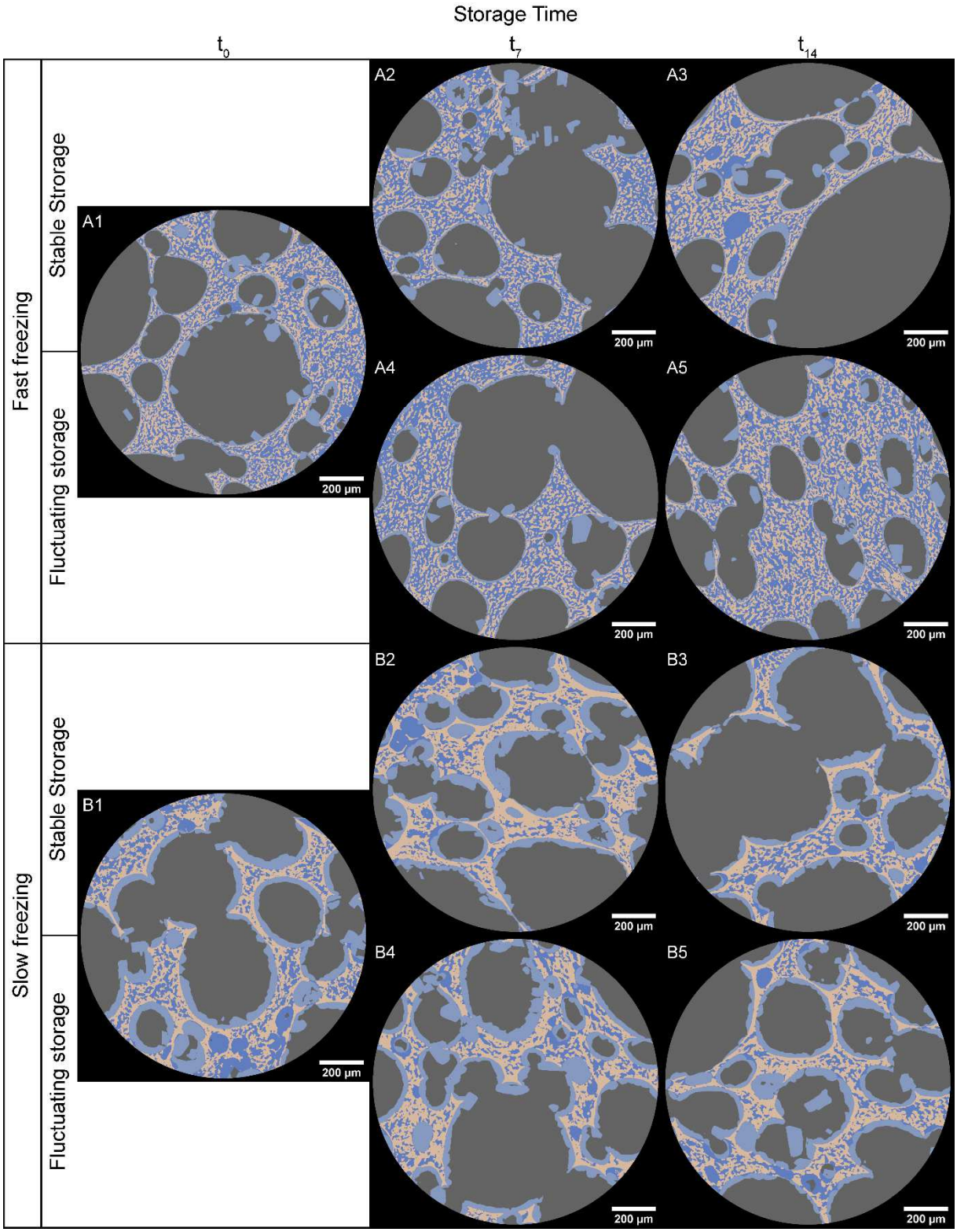

Figure 6: *Synchrotron X-ray µCT slices of the labeled 3D images for the sponge cake samples frozen at (A) fast rate and at (B) slow rate (Air in grey, ice outside the matrix in light blue, ice inside the matrix in dark blue and starch in brown).*

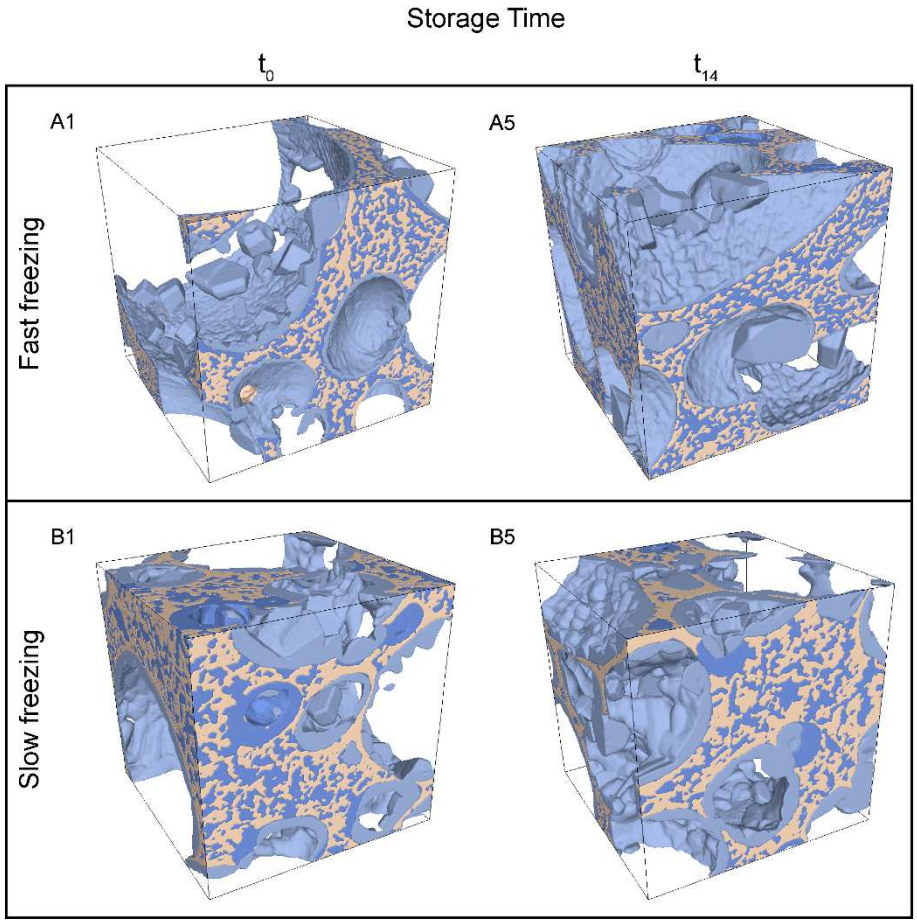

Figure 7: *3D visualization of the segmented Synchrotron X-ray µCT images for the sponge cake samples frozen at (A) fast rate and at (B) slow rate. (Ice outside the matrix in light blue, ice inside the matrix in dark blue and starch in brown). A1, A5, B1 and B5 are the corresponding 3D visualizations of the slices with the same caption in Figure 6. Each cube is 500 µm a side.*

III.2. Quantitative analysis

III.2.1 Volume fractions

Tables 3 summarized the volume fractions computed from the 3D images for the different conditions. These results are also plotted in the Figure 8.

Table 3: *Mean volume fraction of the different phases (air, ice and ice inside) for different conditions.*

Storage conditions	**Storage duration (days)**	**Fast freezing**			**Slow freezing**		
		Air	**Ice**	**Ice inside**	**Air**	**Ice**	**Ice inside**
	0	61.6 ± 4.6^{a}	61.9 ± 0.6^{a}	43.3 ± 2.0^{a}	54.9 ± 2.7^{a}	63.6 ± 0.1^{a}	24.1 ± 1.0^{a}
Stable storage	7	59.5 ± 8.1^{a}	62.6 ± 1.2^{a}	41.2 ± 2.7^{a}	62.3 ± 2.2^{b}	63.9 ± 0.5^{a}	24.5 ± 6.3^{a}
	14	64.4 ± 4.1^{a}	62.6 ± 1.0^{a}	42.7 ± 2.8^{a}	66.3 ± 4.5^{b}	63.7 ± 1.2^{a}	21.4 ± 1.5^{b}
Fluctuating storage	7	62.2 ± 2.2^{a}	61.9 ± 0.3^{a}	42.0 ± 0.8^{a}	53.5 ± 4.9^{a}	64.6 ± 1.6^{a}	27.2 ± 4.3^{c}
	14	64.9 ± 4.7^{a}	63.1 ± 1.1^{a}	42.0 ± 2.6^{a}	63.0 ± 3.9^{b}	64.1 ± 0.3^{a}	22.0 ± 1.0^{b}

Comparisons were made between data in the same column. A same index letter indicate that there is no significant differences between values within a single column, $p > 0.05$.

Overall, it is noteworthy that the air volume fractions obtained by image analysis and presented in Table 3 and Figure 8 are in line with the mean porosity value (56 ± 2 %) determined by experimental measurements (see Table 2). However, significant differences ($p < 0.05$) were obtained for air volume fractions at slow freezing rate whatever storage condition and duration, while there was no significant difference ($p > 0.05$) at fast freezing rate. These differences may be related to the local heterogeneity of the initial porosity of the sample as shown in our previous work (Zennoune et al. 2021). Indeed, it was reported that the model sponge cake has a multiple scale porosity that is heterogeneously distributed, making the sample porosity greatly dependent on the sampling location.

Table 3 and Figure 8 also show that the total ice volume fractions are similar (about 60%) whatever the freezing rate, the storage condition and storage duration. However, the ice location is different according to the freezing rate. The mean volume fraction of ice inside the matrix obtained for fast freezing is higher (quite twice) than the one found for slow freezing, corresponding to almost two thirds of the total ice formed. Inversely, for slow freezing, two thirds of the total ice are mainly formed at the air-starch interface. These quantitative results are consistent with the observations described in Figures 6A1, 6B1, 7A1 and 7B1 and with the physical phenomena occurring at the initial state, that was also described in our previous work (Zennoune et al. 2021).

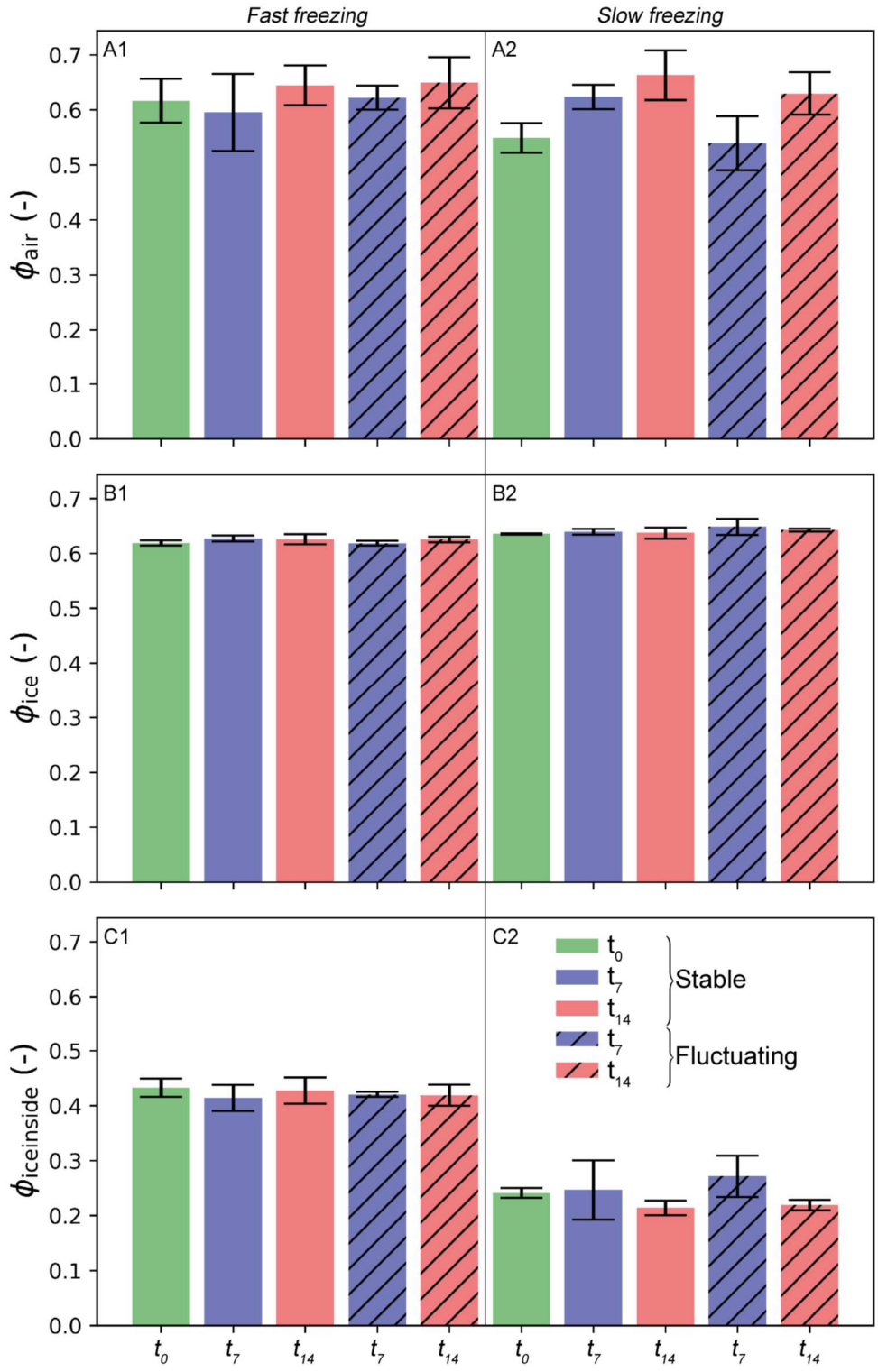

Figure 8: *Volume fractions of (A) air, (B) ice and (C) ice inside the matrix. (A1,B1,C1) for samples obtained in the fast freezing conditions; (A2,B2,C2) for samples obtained in the slow freezing conditions.*

III.2.2 Specific surface area and local thickness

Considering the SSA values shown in Table 4 and Figure 9, significant differences were obtained for both air/ice and ice/starch interfaces. The SSA values can be related to the local thickness distributions of ice as shown in Figure 10. The standard deviations of the distributions are represented by the shaded areas in Figure 10.

Table 4: *Specific Surface Area (mm^{-1}).*

Storage conditions	**Storage duration (days)**	**Fast freezing**		**Slow freezing**	
		$SSA_{air/ice}$	$SSA_{ice/starch}$	$SSA_{air/ice}$	$SSA_{ice/starch}$
	0	8.0 ± 0.9^{a}	50.0 ± 9.7^{a}	7.7 ± 1.0^{a}	27.0 ± 3.0^{a}
Stable storage	7	8.6 ± 2.4^{a}	45.2 ± 14.9^{a}	8.5 ± 3.4^{a}	23.4 ± 7.1^{a}
	14	7.4 ± 1.7^{a}	38.6 ± 9.5^{b}	8.0 ± 2.0^{a}	18.6 ± 5.4^{b}
Fluctuating storage	7	7.9 ± 0.4^{a}	48.5 ± 5.3^{a}	7.7 ± 0.7^{a}	26.1 ± 2.9^{a}
	14	8.7 ± 1.0^{b}	46.3 ± 4.9^{c}	8.7 ± 0.4^{b}	21.0 ± 4.7^{c}

Comparisons were made between data in the same column. A same index letter indicate that there is no significant differences between values within a single column, $p > 0.05$.

<u>For fast frozen samples:</u>

- Table 4 and Figure 9A1 show that the $SSA_{air/ice}$ exhibit values between 7.4 mm^{-1} (stable storage - t_{14}) and 8.7 mm^{-1} (fluctuating storage - t_{14}). In the case of a fluctuating storage, the $SSA_{air/ice}$ increases significantly ($p < 0.05$) with the storage duration. This can be due to an increase of the roughness of the ice layer or by the growth of individual crystals at the interface. This seems to be confirmed by the evolution of the local thickness of the ice outside presented in Figure 10. Indeed, it can be observed on Figures 10A2, B2 and C2, in the case of a fluctuating storage, that the local thickness of the ice outside increases with the storage duration: at t_0, the maximum local thickness (for 99% of ice) is nearly 47 µm whereas it is 63 µm and 70 µm at time t_7 and t_{14}, respectively. It means that, locally, a part of the ice layer has grown leading to a coarser and heterogeneous ice surface. By contrast, in the case of a stable storage, there is no evident trend for the $SSA_{air/ice}$ mostly because of the high standard deviations (Table 4 and Figure 9A1). This may represent an increasing heterogeneity between and within the samples with increasing storage duration.

- The $SSA_{ice/starch}$ ranges between 50.0 mm^{-1} (for t_0) and 38.6 mm^{-1} (stable storage - t_{14}) (Table 4 and Figure 9B1). The $SSA_{ice/starch}$ values tend to decrease with the storage duration regardless the storage conditions (stable or fluctuating). This decrease of the surface between the ice inside and the starch, which is more pronounced in the case of the stable condition, reflects probably a decrease in the number of small crystals and a growth of the larger ice crystals. Indeed, in the case of a stable storage Figures 10A1, B1 and C1 show that at t_0, the maximum local thickness of the ice inside is 20 µm for more than 99% of ice volume whereas it is 50 µm at t_{14}.

<u>For slow frozen samples</u>:

- The $SSA_{air/ice}$ ranges between 7.7 mm^{-1} (at t_0) and 8.7 mm^{-1} (at t_{14} - fluctuating storage) as can be seen in Table 4 and Figure 9A2. As for the fast frozen samples, the $SSA_{air/ice}$ increases slightly with the storage duration in the case of temperature fluctuations. Similarly, there is no clear trend in the case of a stable temperature storage, which shows large standard deviations.

- The $SSA_{ice/starch}$ values vary between 27 mm^{-1} (at t_0) and 18.6 mm^{-1} (at t_{14} - stable storage) as shown in Table 4 and Figure 9B2. It can be seen a clear decrease the $SSA_{ice/starch}$ values with the storage duration whatever the storage conditions. Once again, this decrease is more pronounced in the case of stable storage temperatures. It can also correspond to a growth in the size of ice crystals, even if this increase is not well pronounced on the local thickness values in Figure 10A1, B1 and C1.

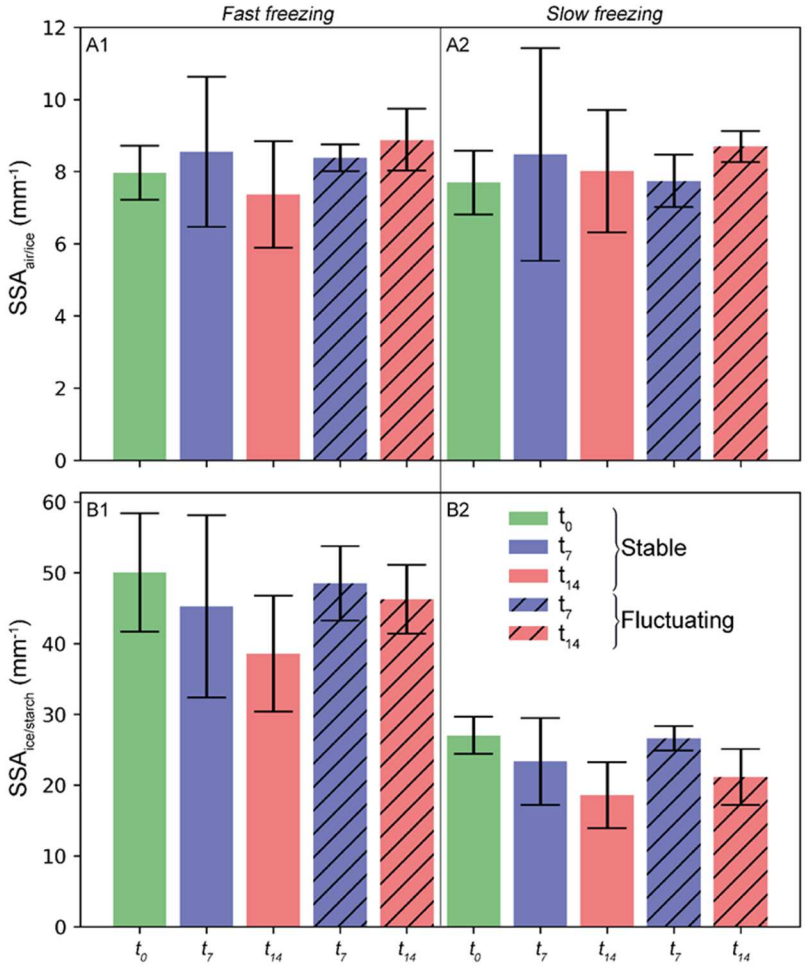

Figure 9: *(A) Specific Surface Area of the air/ice interface $SSA_{air/ice}$ (B) Specific Surface Area of the ice/starch interface $SSA_{ice/starch}$. (A1, B1) for samples obtained in the fast freezing conditions and (A2, B2) for samples obtained in the slow freezing conditions.*

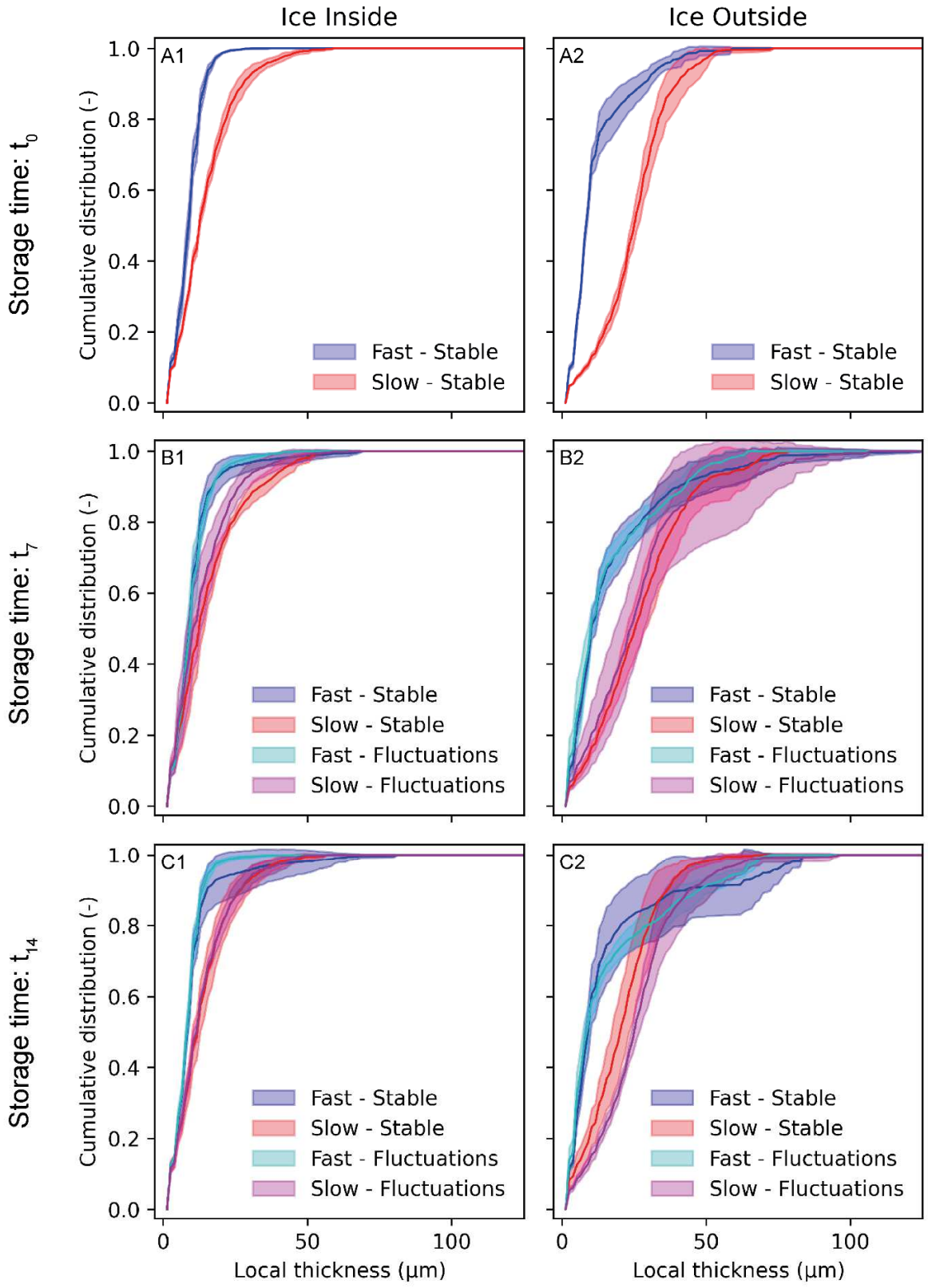

448

449 ***Figure 10:*** *Cumulative distribution of local thickness of. (1) ice inside the matrix and (2) ice outside*
450 *the matrix after (A) freezing, (B) 7 days of storage and (C) 14 days of storage, both for stable and*
451 *fluctuating storage temperatures. The standard deviations of the distributions are represented by the*
452 *shaded areas.*

IV. Discussion

IV.1. Water migration and redistribution

Sponge cake samples were visualized using synchrotron X-ray µCT. The samples were first frozen at two different freezing rates (fast and slow freezing). Figures 6A1, 6B1, 7A1 and 7B1 clearly evidenced that the freezing rate has an impact on ice formation and location. Fast freezing leads to the formation of numerous small ice crystals homogenously distributed inside the matrix and to a thin ice layer at the pore walls while slow freezing leads to the formation of bigger ice crystals heterogeneously distributed and to a thick ice layer at the pore surface. In addition, the volume fractions of ice inside the matrix (43.3 ± 2.0 % for fast freezing and 24.1 ± 1.0 % for slow freezing) and $SSA_{ice/starch}$ (50.0 ± 9.7 mm $^{-1}$ for fast freezing and 27.0 ± 3.0 mm^{-1} for slow freezing) displayed in Table 3 and Table 4, respectively, highlights a second finding. They show that ice was mainly formed inside the matrix when the product was frozen quickly whereas it was largely located inside the pores for slow freezing. This corroborates our earlier reports (Zennoune et al. 2021) in which we argued that both nucleation and ice crystal growth are controlled by the freezing rate through heat transfer (thermal resistance) and moisture transfer (freezable water diffusion). In addition, the high porosity of the model sponge cake affects water mobility and ice distribution during freezing. On the one hand, the fast freezing rate favors the creation of ice nuclei with low critical size but limits the water diffusion for ice crystal growth and towards the pores, leading thus to the formation of numerous small ice crystals, especially inside the matrix. On the other hand, during slow freezing, the nucleation phenomenon is limited due to the high critical size of nuclei, but water has enough time to diffuse through the matrix and towards the pores, resulting in fewer but large ice crystals inside the matrix and a thick ice layer at the pores walls.

After freezing, both quickly and slowly frozen samples were stored at two different conditions (stable and fluctuating temperatures) for two weeks.

In the case of fast freezing, comparison of images of Figures 6A1 to A5 and Figures 7A1 and A2 reveals that both ice morphology and size seem to evolve with storage time, even though ice distribution inside and outside the matrix seem to be the same. Moreover, this evolution is more noticeable for stable storage temperature than for fluctuating temperature. These observations are in line with the evolutions of both the volume fractions of the ice inside the matrix (Table 3) and the $SSA_{ice/starch}$ (Table 4). As a matter of fact, volume fractions of the ice inside did not vary significantly with storage time and storage temperature conditions (Table 3, $p > 0.05$) while the $SSA_{ice/starch}$ significantly decreases with storage time whatever the storage condition (Table 4, $p < 0.05$). These results show that ice migration from the starch matrix towards the pores is limited or inexistent under these conditions. Instead, a local redistribution of water within the starch matrix seems to happen, resulting in crystal enlargement and crystal number decrease accompanied by mass conservation. This result may be explained by recrystallization phenomena driven by differences in the stability of ice crystals as a function of their size. In the case of fast freezing, the crystalline system is mainly constituted of small crystals, which have high free surface energy and are energetically unstable. Therefore, the system will tend towards a lower energy state by forming larger ice crystals that are more stable.

Given the evolution of the ice inside the starch matrix, several recrystallization mechanisms may occur. These include, at first, recrystallization by accretion when two crystals are close enough to form a bridge and then grow into a single crystal. Then, Ostwald ripening may happen involving water molecules of the small ice crystals to detach gradually from the ice crystal surface and diffuse through the matrix before deposition on larger ice crystals, leading to a decrease in the number of small crystals and a growth of the larger ones.

Still in the case of fast freezing, it is noteworthy that the growth of ice crystal size inside the matrix with storage time is more pronounced for stable storage than for fluctuating storage condition. Indeed, Table 4 shows a high decrease of the $SSA_{ice/starch}$ for stable storage (about −23% from t_0 to t_{14}) compared to that for fluctuating storage (about −7% from t_0 to t_{14}). This result is confirmed by the local thickness analysis. In fact, measured local thicknesses of ice inside the matrix show a larger increase of ice crystal size for stable storage than for fluctuating storage condition. This result is not intuitive, given that it is well recognized that temperature fluctuations promote recrystallization and therefore crystal growth (Donhowe and Hartel 1996a, Donhowe and Hartel 1996b, Ndoye and Alvarez 2015). An explanation might be related to the heat transfers inside the starch matrix. Indeed, the fluctuation duration (1h at −5°C) may not be sufficient to significantly affect the microstructure inside the starch matrix. On the other hand, the fluctuating storage temperature seems to affect the evolution of ice outside the starch matrix (ice inside the pores). The local thickness of ice outside the matrix exhibits a noticeable increase with storage duration for fluctuating storage condition, while the evolution is less pronounced for stable storage condition (Figure 10B2 and C2). This trend is supported by the evolution of the $SSA_{air/ice}$, which is larger for fluctuating storage, compared to stable storage conditions after 14 days of storage (Table 4). These results reveal an increase of the ice layer at the pore interface. Local water redistribution and ice resizing rather than ice migration, keeping in mind that no variation of ice volume fraction was observed (Table 3), can plausibly explain this ice size increase. Unlike the matrix, the pore phase is affected by temperature fluctuations which may favor migratory recrystallization (Ostwald ripening) at the pore interface by a sublimation-diffusion-condensation mechanism leading to larger ice crystal size and to a more stable state.

In the case of slow freezing, visual observations in Figures 6B1 to B5 and Figures 7B1 and B5 show no discernible difference in the microstructure evolution with storage time for both stable and fluctuating storage scenarios. These observations are not in line with the changes of the volume fractions of ice crystals inside the matrix (Table 3), of the $SSA_{ice/starch}$ (Table 4) and of the local thicknesses (Figure 10) during storage, for both storage conditions. Volume fractions of ice inside the matrix decreased significantly after 14 days ($p < 0.05$) when the storage duration increase for stable as well as for fluctuating storage temperatures. Moreover, the $SSA_{ice/starch}$ exhibit large decreases with storage time both for stable (nearly −30 % from t_0 to t_{14}) and fluctuating (around −20 % from t_0 to t_{14}) conditions. In addition, the increase of $SSA_{air/ice}$ values both for stable (about + 4 % from t_0 to t_{14}) and for fluctuating (around +13 % from t_0 to t_{14}) temperatures reveals ice size increase at the pore interfaces. These results reflect, at the same time, the decrease in the number of small ice crystals and the growth of large ice crystals inside the starch matrix and locally ice layer increase at the pore surface. On another note, these results are underpinned by the increase of local thickness with storage time both inside and

outside the matrix. Two hypotheses can be put forward to explain these findings: *(i)* a migration of water from the matrix to the pores where it is deposited on the starch surface or on the existing ice layer by sublimation-diffusion-condensation phenomenon (Ostwald ripening); *(ii)* a local redistribution of water in the matrix through recrystallization phenomena (mainly Ostwald ripening) leading to an enlargement of the ice crystals. The first hypothesis may explain both the decrease of ice volume fractions inside the matrix and the increase of the ice characteristic size in the pores after 14 days. The second hypothesis can plausibly explain the ice crystal growth inside the starch matrix. Local redistribution inside the starch matrix seems to be more important at stable temperature storage while water migration from the matrix towards the pores appears to be predominant in the case of fluctuating storage conditions. Chen et al. (2013) reported that during long-term storage significant water redistribution was noticed. This redistribution was accompanied by ice recrystallization and growth. Similar results were found by Eckardt et al. (2013) who studied bread and dough and by Kontogiorgos and Goff (2006) who studied flour-water mixture. In both cases, the authors explained ice crystal growth by recrystallization resulting in the destruction of the microstructure.

IV.2. Coupled effect of freezing rates and frozen storage conditions

As mentioned previously, fast and slow freezing of the model sponge cake give rise to, respectively, small and coarse ice crystals inside the starch matrix. At the same time, more or less ice layer is formed at the pore interfaces depending on the freezing rate. In the case of slow freezing, the majority of the ice is formed at these pore interfaces reflecting a greater water migration from the matrix towards the pores. During frozen storage, the crystalline microstructure evolves regardless of the initial freezing rate and the storage conditions. However, the changes in microstructure are more significant when the products are slowly-frozen as evidenced by the larger decrease of the $SSA_{ice/starch}$ compared to fast freezing (Table 4). This means that when the same storage conditions are applied, ice crystals grow more in sponge cake frozen at slow freezing rate. This result is confirmed by the local thickness values depicted in Figure 10. For both ice locations (inside and outside the matrix), local thickness values are always higher for slow freezing than for fast freezing and for the three time points (t_0, t_7 and t_{14}). As mentioned above, local water redistribution and ice resizing by recrystallization mechanisms are favored in fast frozen samples while water migration is added to the local redistribution in slowly frozen samples, explaining the greater changes observed in the latter. It is noteworthy that coupling fast freezing with poor storage conditions (fluctuating temperatures) leads to smaller ice crystals and less damage to the microstructure than combining slow freezing with good storage conditions (stable temperatures). This result can be explained by the fact that fast freezing initially leads to a more homogeneous ice crystal population than slow freezing. It is well known that homogeneous population is energetically more stable than heterogeneous population and therefore is less likely to undergo ice recrystallization (Hartel 1998, Kobayashi et al. 2018).

Moreover, it is important to point out that microstructural changes affect the texture of the sponge cake and consequently its quality. This impact is more pronounced as the size of the ice crystals is bigger. Under the conditions used in this study, the benefits of fast freezing are

reduced at the end of the two-week storage period, but the products still have a better quality than slowly-frozen samples. To our knowledge, such results about the combined effect of freezing and frozen storage conditions are reported for the first time. The combined effects of freezing rate and storage time and temperature on the quality of frozen porous foods was studied for bread dough and bread (Yi and Kerr 2009, Eckardt et al. 2013) and for sponge cake (Díaz-Ramírez et al. 2016, Van Bockstaele et al. 2021). However, none of these works has investigated pore and ice crystal evolution as impacted by the coupled freezing and frozen storage processes.

V. Conclusion

Freezing and frozen storage of sponge cake have an impact on ice formation and growth which can cause undesirable changes to the product. In this article, the impact of freezing rate and storage conditions on ice formation and location was studied. The analysis of synchrotron µCT images leads to the conclusion that the ice volume fraction (about 60%) obtained after freezing is conserved during frozen storage, whatever the storage conditions. However, ice redistribution and relocation occur during storage depending on both initial freezing and frozen storage conditions, as shown by the evolutions of volume fraction of ice inside the matrix, and the SSA values. During the whole storage period, slow freezing gives rise to a decrease of the volume fraction of ice inside the matrix (up to −13%) combined to the $SSA_{ice/starch}$ values drop (up to −30%) and the $SSA_{air/ice}$ values increase (up to +13%) meaning ice local redistribution and ice migration from the matrix to pores. For fast freezing, no change in ice inside volume fraction was noticed, but the $SSA_{ice/starch}$ values decreased (up to −23%) and the $SSA_{air/ice}$ values increased (up to +11%) evidencing a local redistribution of ice both inside the matrix and in the pores without migration towards the pores. It was shown that fast freezing causes less microstructural changes, regardless of the storage conditions, even though the microstructure continues to evolve during frozen storage, due to ice migration and recrystallization.

Before this study, the mechanism of ice formation in porous foods according to the freezing process, as well as the mechanism of pore and ice crystal evolution during frozen storage were poorly understood. This work is an important step forward, but further investigations are still needed. For example, the impact of temperature fluctuations was not clearly evidenced, especially inside the starch matrix. It would be of interest to study the impact of more aggressive fluctuations to bring a better knowledge of the influence of temperature fluctuation. Another limitation of this study is related to the fact that each sample is different, even if their mean porosity and water content was similar. Following the microstructural evolution of the same sample during freezing and storage should limit the effect of heterogeneity arising from the sampling location in the sponge cake. In addition, it would be useful to formalize the link between the evolution of the microstructure and the classical quality criteria such as texture or drip loss.

The freezing process and the frozen storage are the main components of the frozen cold chain. A better understanding of the mechanisms involved during these two steps would be very useful

for a better control of microstructure and induced quality changes of frozen products throughout the cold chain.

Acknowledgments

We would like to thank Alain Denis from UR FRISE INRAE for his technical help. We acknowledge SOLEIL for provision of synchrotron radiation facilities on ANATOMIX and financial support concerning the proposal study number 20200227. ANATOMIX is an Equipment of Excellence (EQUIPEX) funded by the *Investments for the Future* program of the French National Research Agency (ANR), project *NanoimagesX*, grant no. ANR-11-EQPX-0031. The authors would like to thank Guillaume Daniel of the ANATOMIX team for technical support at the beamline. We acknowledge also CNRM/CEN which is part of the LabEx OSUG@2020 (*Investments for the Future* program, grant agreement ANR10 LABX56) and 3SR Laboratory which is part of the LabEx Tec21 (*Investments for the Future* program, grant agreement ANR11 LABX0030).

Conflict of Interest: The authors declare no conflict of interest. The funders had no role in the design of the study; in the collection, analyses, or interpretation of data; in the writing of the manuscript, or in the decision to publish the results.

References

Alizadeh, E., Chapleau, N., de Lamballerie, M. and Le-Bail, A. (2007). *Effect of different freezing processes on the microstructure of Atlantic salmon (Salmo salar) fillets*. Innovative Food Science & Emerging Technologies, 8(4): 493-499.

Anese, M., Mirolo, G., Beraldo, P. and Lippe, G. (2013). *Effect of ultrasound treatments of tomato pulp on microstructure and lycopene in vitro bioaccessibility*. Food chemistry, 136(2): 458-463.

Baier-Schenk, A., Handschin, S. and Conde-Petit, B. (2005). *Ice in prefermented frozen bread dough—an investigation based on calorimetry and microscopy*. Cereal Chemistry, 82(3): 251-255.

Ban, C., Yoon, S., Han, J., Kim, S. O., Han, J. S., Lim, S. and Choi, Y. J. (2016). *Effects of freezing rate and terminal freezing temperature on frozen croissant dough quality*. Lwt-Food Science and Technology, 73: 219-225.

Bárcenas, M. a. E., Benedito, C. and Rosell, C. M. (2004). *Use of hydrocolloids as bread improvers in interrupted baking process with frozen storage*. Food Hydrocolloids, 18(5): 769-774.

Bárcenas, M. E. and Rosell, C. M. (2006). *Effect of frozen storage time on the bread crumb and aging of par-baked bread*. Food Chemistry, 95(3): 438-445.

Bevilacqua, A., Zaritzky, N. and Calvelo, A. (1979). *Histological measurements of ice in frozen beef*. International Journal of Food Science & Technology, 14(3): 237-251.

Bousquières, J. (2017). *Impact de la composition et des procédés sur la réactivité d'un produit modèle alvéolé de type cake*, Université Paris-Saclay.

Brownlee, K. A. (1965). Statistical theory and methodology in science and engineering. New York, John Wiley and Sons.

Calonne, N., Flin, F., Geindreau, C., Lesaffre, B. and Rolland du Roscoat, S. (2014). *Study of a temperature gradient metamorphism of snow from 3-D images: time evolution of microstructures, physical properties and their associated anisotropy*. The Cryosphere, 8(6): 2255-2274.

Calonne, N., Flin, F., Lesaffre, B., Dufour, A., Roulle, J., Puglièse, P., Philip, A., Lahoucine, F., Geindreau, C., Panel, J.-M., du Roscoat, S. R. and Charrier, P. (2015). *CellDyM: A room temperature operating cryogenic cell for the dynamic monitoring of snow metamorphism by time-lapse X-ray microtomography*. Geophysical Research Letters, 42(10): 3911-3918.

Chassagne-Berces, S., Poirier, C., Devaux, M. F., Fonseca, F., Lahaye, M., Pigorini, G., Girault, C., Marin, M. and Guillon, F. (2009). *Changes in texture, cellular structure and cell wall composition in apple tissue as a result of freezing*. Food Research International, 42(7): 788-797.

Chen, G., Jansson, H., Lustrup, K. F. and Swenson, J. (2012). *Formation and distribution of ice upon freezing of different formulations of wheat bread*. Journal of Cereal Science, 55(3): 279-284.

Chen, G., Öhgren, C., Langton, M., Lustrup, K. F., Nydén, M. and Swenson, J. (2013). *Impact of long-term frozen storage on the dynamics of water and ice in wheat bread*. Journal of cereal science, 57(1): 120-124.

Díaz-Ramírez, M., Calderón-Domínguez, G., Salgado-Cruz, M. d. l. P., Chanona-Pérez, J. J., Andraca-Adame, J. A. and Ribotta, P. D. (2016). *Sponge cake microstructure, starch retrogradation and quality changes during frozen storage*. International Journal of Food Science & Technology, 51(8): 1744-1753.

Donhowe, D. P. and Hartel, R. W. (1996). *Recrystallization of ice during bulk storage of ice cream*. International Dairy Journal, 6(11-12): 1209-1221.

Donhowe, D. P. and Hartel, R. W. (1996a). *Recrystallization of ice in ice cream during controlled accelerated storage*. International Dairy Journal, 6(11): 1191-1208.

Donhowe, D. P. and Hartel, R. W. (1996b). *Recrystallization of ice during bulk storage of ice cream*. International Dairy Journal, 6(11): 1209-1221.

Eckardt, J., Öhgren, C., Alp, A., Ekman, S., Åström, A., Chen, G., Swenson, J., Johansson, D. and Langton, M. (2013). *Long-term frozen storage of wheat bread and dough–Effect of time, temperature and fibre on sensory quality, microstructure and state of water*. Journal of Cereal Science, 57(1): 125-133.

Eckardt, J., Öhgren, C., Alp, A., Ekman, S., Åström, A., Chen, G., Swenson, J., Johansson, D. and Langton, M. (2013). *Long-term frozen storage of wheat bread and dough – Effect of time, temperature and fibre on sensory quality, microstructure and state of water*. Journal of Cereal Science, 57(1): 125-133.
Esselink, E. F., van Aalst, H., Maliepaard, M. and van Duynhoven, J. P. (2003). *Long-term storage effect in frozen dough by spectroscopy and microscopy*. Cereal chemistry, 80(4): 396-403.
Haffar, I., Flin, F., Geindreau, C., Petillon, N., Gervais, P.-C. and Edery, V. (2021). *X-ray tomography for 3D analysis of ice particles in jet A-1 fuel*. Powder Technology, 384: 200-210.
Haffar, I., Flin, F., Geindreau, C., Petillon, N., Gervais, P.-C. and Edery, V. (2022). *3D microstructure evolution of ice in jet A-1 fuel as a function of applied temperature over time*. International Journal of Heat and Mass Transfer, 183: 122158.
Hagiwara, T., Hartel, R. W. and Matsukawa, S. (2006). *Relationship between recrystallization rate of ice crystals in sugar solutions and water mobility in freeze-concentrated matrix*. Food Biophysics, 1(2): 74-82.
Hartel, R. W. (1998). Mechanisms and kinetics of recrystallization in ice cream. The properties of water in foods ISOPOW 6, Springer**:** 287-319.
Kobayashi, R., Kimizuka, N., Suzuki, T., Watanabe, M. and Int Inst, R. (2014). Effect of supercooled freezing methods on ice structure observed by X-ray CT. 3rd Iir International Conference on Sustainability and the Cold Chain. Paris, Int Inst Refrigeration. **2014:** 392-396.
Kobayashi, R., Kimizuka, N., Watanabe, M., Takenaga, F. and Suzuki, T. (2018). *Property Changes during Frozen Storage in Frozen Soy Bean Curds Prepared by Freezing Accompanied with Supercooling*. Transactions of the Japan Society of Refrigerating and Air Conditioning Engineers, 35(3): 269.
Kontogiorgos, V. and Goff, H. D. (2006). *Calorimetric and microstructural investigation of frozen hydrated gluten*. Food Biophysics, 1(4): 202-215.
Legland, D., Arganda-Carreras, I. and Andrey, P. (2016). *MorphoLibJ: integrated library and plugins for mathematical morphology with ImageJ*. Bioinformatics, 32(22): 3532-3534.
Lucas, T., Le Ray, D. and Davenel, A. (2005). *Chilling and freezing of part-baked bread. Part I: An MRI signal analysis*. Journal of food engineering, 70(2): 139-149.
Masselot, V., Bosc, V. and Benkhelifa, H. (2021). *Analyzing the microstructure of a fresh sorbet with X-ray micro-computed tomography: Sampling, acquisition, and image processing*. Journal of Food Engineering, 292: 110347.
Medebacha, A., Pinzera, B. R., Duboisb, C., Limbachb, H. J., Schneebelic, M. and Stampanonia, M. (2013). *X-ray phase contrast tomography of ice cream : A time-lapse study*. Food Symposium. Leuven, Belgium.
Mirone, A., Gouillart, E., Brun, E., Tafforeau, P. and Kieffer, J. (2013). *The PyHST2 hybrid distributed code for high speed tomographic reconstruction with iterative reconstruction and a priori knowledge capabilities*. Nuclear Instruments and Methods in Physics Research Section B Beam Interactions with Materials and Atoms, 324.
Mousavi, R., Miri, T., Cox, P. W. and Fryer, P. J. (2005). *A novel technique for ice crystal visualization in frozen solids using X-ray micro-computed tomography*. Journal of Food Science, 70(7): E437-E442.
Mousavi, R., Miri, T., Cox, P. W. and Fryer, P. J. (2007). *Imaging food freezing using X-ray microtomography*. International Journal of Food Science and Technology, 42(6): 714-727.
Mulot, V. (2019). *Caractérisation expérimentale et modélisation multi-échelles des transferts thermiques et d'eau lors de la congélation des produits alimentaires*, Institut agronomique, vétérinaire et forestier de France.
Mulot, V., Fatou-Toutie, N., Benkhelifa, H., Pathier, D. and Flick, D. (2019). *Investigating the effect of freezing operating conditions on microstructure of frozen minced beef using an innovative X-ray micro-computed tomography method*. Journal of Food Engineering, 262: 13-21.
Ndoye, F. T. and Alvarez, G. (2015). *Characterization of ice recrystallization in ice cream during storage using the focused beam reflectance measurement*. Journal of Food Engineering, 148: 24-34.

Otsu, N. (1979). *A Threshold Selection Method from Gray-Level Histograms*. IEEE Transactions on Systems, Man and Cybernetics, SMC-9(1): 62-66.
Paganin, D., Mayo, S. C., Gureyev, T. E., Miller, P. R. and Wilkins, S. W. (2002). *Simultaneous phase and amplitude extraction from a single defocused image of a homogeneous object*. Journal of microscopy, 206(1): 33-40.
Pham, Q. T. (2006). *Modelling heat and mass transfer in frozen foods: a review*. International Journal of Refrigeration, 29(6): 876-888.
Pinzer, B. R., Medebach, A., Limbach, H. J., Dubois, C., Stampanoni, M. and Schneebeli, M. (2012). *3D-characterization of three-phase systems using X-ray tomography: tracking the microstructural evolution in ice cream*. Soft Matter, 8(17): 4584-4594.
Pronk, P., Ferreira, C. I. and Witkamp, G.-J. (2005). *A dynamic model of Ostwald ripening in ice suspensions*. Journal of Crystal Growth, 275(1-2): e1355-e1361.
Roca, E., Guillard, V., Guilbert, S. and Gontard, N. (2006). *Moisture migration in a cereal composite food at high water activity: Effects of initial porosity and fat content*. Journal of Cereal Science, 43(2): 144-151.
Schindelin, J., Arganda-Carreras, I., Frise, E., Kaynig, V., Longair, M., Pietzsch, T., Preibisch, S., Rueden, C., Saalfeld, S. and Schmid, B. (2012). *Fiji: an open-source platform for biological-image analysis*. Nature methods, 9(7): 676-682.
Silvas-García, M., Ramírez-Wong, B., Torres-Chávez, P., Carvajal-Millan, E., Barrón-Hoyos, J., Bello-Pérez, L. A. and Quintero-Ramos, A. (2014). *Effect of freezing rate and storage time on gluten protein solubility, and dough and bread properties*. Journal of Food Process Engineering, 37(3): 237-247.
Ullah, J., Takhar, P. S. and Sablani, S. S. (2014). *Effect of temperature fluctuations on ice-crystal growth in frozen potatoes during storage*. LWT - Food Science and Technology, 59(2, Part 1): 1186-1190.
Van Bockstaele, F., Debonne, E., De Leyn, I., Wagemans, K. and Eeckhout, M. (2021). *Impact of temporary frozen storage on the safety and quality of four typical Belgian bakery products*. LWT, 137: 110454.
van Dalen, G., Don, A., Nootenboom, P. and C G Blonk, J. (2009). *Determination of bubbles in foods by X-ray microtomography and image analysis*. SkyScan Micro-CT user meeting. Ghent, Belgium**:** 15-23.
van Dalen, G., Koster, M., Nijsse, J., Boller, E. and van Duynhoven, J. (2013). *3D imaging of freeze-dried vegetables using X-ray microtomography*. Micro-CT user meeting SkyScan, Hasselt, Belgium.
Vicent, V., Ndoye, F.-T., Verboven, P., Nicolaï, B. and Alvarez, G. (2019). *Effect of dynamic storage temperatures on the microstructure of frozen carrot imaged using X-ray micro-CT*. Journal of Food Engineering, 246: 232-241.
Vicent, V., Ndoye, F. T., Verboven, P., Nicolai, B. and Alvarez, G. (2016). Applicability of X-ray Microtomography for Characaterizing the microstructure of Frozen Apple during Storage. 4th Iir International Conference on Sustainability and the Cold Chain. A. East, J. Carson, D. Cleland and R. Love. Paris, Int Inst Refrigeration**:** 414-420.
Vicent, V., Verboven, P., Ndoye, F.-T., Alvarez, G. and Nicolaï, B. (2017). *A new method developed to characterize the 3D microstructure of frozen apple using X-ray micro-CT*. Journal of Food Engineering, 212(Supplement C): 154-164.
Voda, A., Homan, N., Witek, M., Duijster, A., van Dalen, G., van der Sman, R., Nijsse, J., van Vliet, L., Van As, H. and van Duynhoven, J. (2012). *The impact of freeze-drying on microstructure and rehydration properties of carrot*. Food Research International, 49(2): 687-693.
Weitkamp, T., Scheel, M., Giorgetta, J., Joyet, V., Le Roux, V., Cauchon, G., Moreno, T., Polack, F., Thompson, A. and Samama, J. (2017). *The tomography beamline ANATOMIX at Synchrotron SOLEIL*. Journal of Physics: Conference Series, IOP Publishing.
Yi, J. and Kerr, W. L. (2009). *Combined effects of freezing rate, storage temperature and time on bread dough and baking properties*. LWT-Food Science and Technology, 42(9): 1474-1483.

Zennoune, A., Latil, P., Ndoye, F.-T., Flin, F., Perrin, J., Geindreau, C. and Benkhelifa, H. (2021). *3D Characterization of Sponge Cake as Affected by Freezing Conditions Using Synchrotron X-ray Microtomography at Negative Temperature*. Foods, 10(12): 2915.
Zhao, Y. and Takhar, P. S. (2017). *Micro X-ray computed tomography and image analysis of frozen potatoes subjected to freeze-thaw cycles*. LWT - Food Science and Technology, 79: 278-286.